

A Model for Interpretation of hyperspectral Remote Sensing Reflectance

Zhongping Lee¹, Kendall L. Carder¹, Steve K. Hawes¹, Robert G. Steward¹,
Thomas G. Peacock¹ and Curtiss O. Davis²

¹ Department of Marine Science

University of South Florida

140 Seventh Avenue South

St. Petersburg, FL 33701

Tel. (813)893-9503

² Jet Propulsion Laboratory, California Institute of

Technology

4800 Oak Grove Blvd.

Pasadena, CA 91109

ABSTRACT

Remote sensing reflectance is easier to interpret for the open ocean than for coastal regions because the optical signals are highly coupled to the phytoplankton (e.g. chlorophyll) concentrations. For estuarine or coastal waters, variable terrigenous CDOM, suspended sediments, and bottom reflectance, factors that do not covary with the pigment concentration confound data interpretation. To estimate the pigment concentration, the water-leaving radiance signal must be corrected for the effects of these non-covarying factors. A two-parameter model is presented to model remote sensing reflectance of the water-column, to which contributions due to bottom reflectance, CDOM fluorescence and water Raman scattering are added. The purpose of this research is to try to understand each of these contributions for stations on the West Florida Shelf and in Lake Tahoe. The model requires data with spectral resolution of 10 nm or better, consistent with that provided by the Airborne Visible and InfraRed Imaging Spectrometer (AVIRIS) and expected from the High Resolution Imaging Spectrometer (HIRIS).

1. INTRODUCTION

The use of the power-law of spectral radiance ratios^{1,2} to measure pigment concentrations requires that the water-leaving radiance be largely determined by variations in the pigment concentration, with all other optical constituents covarying along with this quantity. The method works quite well for the open ocean or "Case I" waters³. This is in part because the water-

leaving radiance of open-ocean waters is not affected by bottom reflectance, land run-off, and suspended sediments. Although aeolian dust may be carried by winds to the open ocean⁴, the dominant effect of the particulates may still derive from phytoplankton⁵.

The power-law approach can be much less accurate for estuarine and/or coastal areas⁶, however, because many of the optical constituents are independent of phytoplankton concentrations. In these areas, the water-leaving radiance may include not only parts due to elastic scattering by water molecules, phytoplankton detritus, suspended particulates, bottom reflectance, but it may also include the in-elastic scattering of CDOM fluorescence and water Raman scattering. Thus, changes in ocean color due to suspended sediments or dissolved organic matter may be falsely interpreted as changes in pigment concentration^{6,7}. How the above components influence the power-law is not known very clearly.

It is important to have a good estimate of the pigment concentration for the coastal area since the shelf and slope regions provide about half of the ocean primary production⁸. For open ocean areas, good estimates of primary production based upon CZCS-derived pigment concentration have been obtained^{5,7}.

For water depth measurements^{9,10} or bottom-feature mapping¹¹, water-leaving radiance or irradiance is usually considered to be due to scattering by water molecules, particulates and the bottom, but not due to contributions from the CDOM fluorescence and water Raman. The accurate quantification of pigment concentration, water depth, and/or sea grass maps depends

on how well we understand all of the contributions to the water-leaving radiance and/or irradiance, however. As an initial attempt to interpret remote sensing reflectance data including effects from all major sources, this work considers the separate contributions of the above components using high-spectral-resolution data.

2. THEORY

The upwelling radiance leaving the ocean is a complicated mix of signals due to many components. The major contributions arise from the following: absorption by molecules and particulates, elastic scattering by molecules and particulates, and bottom reflectance for shallow waters. Also included are in-elastic scattering due to water, CDOM, chl-a and phycoerythrin molecules. Since chl-a fluorescence occurs in a narrow band and centered around 685nm, it provides an obvious deviation between measured and modeled remote sensing reflectance (R_{rs}) at 685nm if this emission is not considered in the model. Contributions by Gordon¹² and Carder and Steward¹³ dealing with chl-a fluorescence have been reported and are not directly considered in this work, due to the small signals found in waters with chl-a less than about 1 mg m⁻¹.

It is assumed that the water-leaving radiance (L_u) is composed of the following four components: elastic scattering from molecules and particles (L_{uw}), bottom reflectance (L_{ub}), CDOM fluorescence (L_{uf}), and Raman scattering (L_{uR}). It is also assumed to first order that there are no interactions among these components, so the water-leaving radiance can be expressed as

$$L_u(+,\lambda) = L_{uw}(+,\lambda) + L_{ub}(+,\lambda) + L_{uf}(+,\lambda) + L_{uR}(+,\lambda) \quad (1)$$

The symbols and definitions used in this paper are summarized in Table 1.

The remote sensing reflectance is defined as the ratio of the water-leaving radiance to the downwelling solar irradiance at 0^+m , just above the water surface,

$$R_{rs}(\lambda) = \frac{L_u(0^+, \lambda)}{E_d(0^+, \lambda)} \quad (2)$$

Breaking this equation into contributions from the various mechanisms listed in Eq.1, we have

$$R_{rs}(\lambda) = R_{rsw}(\lambda) + R_{rsb}(\lambda) + R_{rsf}(\lambda) + R_{rsR}(\lambda) \quad (3)$$

For a homogeneous and very deep water body, consider a wavelength-independent factor I to describe the influence of the air-sea interface on the remote sensing reflectance. $R_{rsw}(\lambda)$ can be described in terms of values just below the interface as

$$R_{rsw}(\lambda) = I * \frac{L_{uw}(0^-, \lambda)}{E_d(0^-, \lambda)} \quad (4)$$

where, $I = t_+ * t_- / n^2$, where t is the transmittance of the air-sea interface, subscript "+" indicates a upward flux, subscript "-" indicates an downward flux, and n is the refractive index of water. For a zenith sun, a nadir-viewing instrument and a calm surface, $I \simeq 0.533$. For larger solar zenith angles and foam-covered seas, t will be lower¹⁴.

The subsurface irradiance reflectance due to the water column $R_w(-,\lambda)$ is defined as the ratio of the sub-surface upwelling irradiance to the sub-surface downwelling irradiance:

$$R_w(-, \lambda) = \frac{E_{uw}(0^-, \lambda)}{E_d(0^-, \lambda)} \quad (5)$$

and Austin¹⁴ has related $E_{uw}(-, \lambda)$ and $L_{uw}(-, \lambda)$ through the "Q factor" as

$$Q = \frac{E_{uw}(0^-, \lambda)}{L_{uw}(0^-, \lambda)} \quad (6)$$

so, $R_{rsw}(\lambda)$ can be expressed as

$$R_{rsw}(\lambda) = \frac{I}{Q} * R_w(-, \lambda) \quad (7)$$

For irradiance reflectance $R_w(-, \lambda)$, Górdon et al¹⁵ developed a series relation by the Monte Carlo method

$$R_w(-, \lambda) = \sum_{n=0}^3 \gamma_n \left(\frac{b_b(\lambda)}{a(\lambda) + b_b(\lambda)} \right)^n \quad (8)$$

This equation was simplified^{16,17} to

$$R_w(-, \lambda) \doteq 0.33 * \frac{b_b(\lambda)}{a(\lambda)} \quad (9)$$

for $b_b(\lambda)/a(\lambda)$ values up to ~ 0.25 . The constant 0.33 actually varies slightly with solar zenith angle according to Kirk¹⁸ and Morel and Gentili¹⁹. Since this paper deals with remote sensing reflectance, which is less influenced by the fraction of forward scatter that upwells at solar zenith angle $> 0^\circ$, and R_{rs} will not be as sensitive to sun angle as irradiance reflectance. Thus, we retain 0.33 as a constant, inbed any sun-angle influence to the Q factor as in Appendix, and

proceed.

The total backscattering coefficient, $b_b(\lambda)$, includes two components: backscattering by molecules $b_{bm}(\lambda)$ and particulate matter $b_{bp}(\lambda)$. The total absorption coefficient $a(\lambda)$ includes contributions due to pure sea water absorption $a_w(\lambda)$, gelbstoff or Colored Dissolved Organic Matter (CDOM) absorption $a_g(\lambda)$ and particulate absorption $a_p(\lambda)$. Inserting these into Eq.9 and suppressing the spectral dependence for convenience, we can write $R_{rsw}(\lambda)$ as

$$R_{rsw} = \frac{0.33I}{a_w + a_g + a_p} * \frac{b_{bm} + b_{bp}}{Q} \quad (10)$$

Eq.10 pertains to optically deep water. When optically shallow water is encountered, the reduced scattering by the water column should be considered. Then

$$R_{rsw} = \frac{0.33I}{a} * \frac{b_{bm} + b_{bp}}{Q} * [1 - e^{-(K_d + K_u) * H}] \quad (11)$$

for a totally absorbing bottom and water depth H .

If we define the semi-diffuse attenuation coefficient as $\kappa = a + b_b$, then $K_d = D_d \kappa$ and $K_u = D_u \kappa$. D_d and D_u are the distribution functions for the downwelling and upwelling radiance field and are considered depth-independent, and $D_u/D_d \simeq 2$ according to Gordon et al.¹⁵

The remote sensing reflectance contributions from the bottom reflectance is defined as

$R_{rsb} = L_{ub}(0^+)/E_d(0^+)$. Assuming the bottom is Lambertian, with a reflectance $\rho(\lambda)$, then R_{rsb} can be approximated as

$$R_{rsb} = \frac{I}{\pi} \rho * e^{-(K_d + k) * H} \quad (12)$$

where k is the effective attenuation coefficient for the radiance from a Lambertian source and is approximated as $k \simeq 1.5a$ for vertical radiance²⁰.

The remote sensing reflectance due to gelbstoff or CDOM fluorescence and water Raman are defined as $R_{rsf} = L_{uf}(0^+)/E_d(0^+)$ and $R_{rsR} = L_{uR}(0^+)/E_d(0^+)$. In general, these terms are due to in-elastic scattering (indicated by the subscript I) by CDOM molecules and water molecules. Defining the volume scattering function $\beta_I(\alpha, \lambda_x, \lambda)$ for in-elastic scattering as

$$\beta_I(\alpha, \lambda_x, \lambda) = \frac{T(\alpha, \lambda)}{dV * E(\lambda_x)} \quad (13)$$

where $T(\alpha, \lambda)$ is the intensity of the scattered output radiance, dV is the scattering volume, $E(\lambda_x)$ is the irradiance of the input collimated beam, and α is the angle between the input and the output photon directions.

For z positive downward from the surface, θ is the zenith observational angle, and ψ is the azimuthal observation angle (Fig. 6). To the first order, with the consideration of isotropic β_I , the in-elastic radiance in the direction θ and the upwelling irradiance at depth z due to the depth interval dz are simplified to

$$dL_{uI}(z, \theta, \lambda) = \int_{\lambda_x} \beta_I(\lambda_x, \lambda) * E_0(z, \lambda_x) * d\lambda_x * \frac{dz}{\cos(\theta)} \quad (14)$$

$$dE_{uI}(z, \lambda) = 2\pi \int_{\pi/2}^{\pi} dL_I(z, \theta, \lambda) * \cos(\theta) * \sin(\theta) * d\theta \quad (15)$$

$$= 2\pi \int_{\lambda_x} \beta_I(\lambda_x, \lambda) * E_0(z, \lambda_x) * d\lambda_x * dz \quad (16)$$

where $E_0(z, \lambda_x)$ is the scalar irradiance at depth z , $dV = 1m^2 * dz$, and $E_0(z, \lambda_x) = E_{0d}(z, \lambda_x) + E_{0u}(z, \lambda_x) \simeq D_d(1 + 2R(\lambda_x))E_d(z, \lambda_x)$. Since $E_d(z, \lambda_x) = E_d(0, \lambda_x) * e^{-K_d * z}$, and the upward attenuation coefficient is K_u , then with the consideration that D_d , D_u and the irradiance reflectance R are depth and wavelength-independent, the sub-surface irradiance due to the in-elastic scattering for an infinitely deep water column is

$$E_{uI}(0^-, \lambda) \doteq 2\pi(D_d + D_u R) \int_{\lambda_x} \frac{\beta_I(\lambda_x, \lambda) E_d(0^-, \lambda_x)}{K_u(\lambda) + K_d(\lambda_x)} d\lambda_x \quad (17)$$

Defining Q_I as the Q factor for the in-elastic scattering field, the subsurface radiance due to in-elastic scattering is

$$L_{uI}(0^-, \lambda) \doteq \frac{2\pi(1+2R)}{Q_I} \int_{\lambda_x} \frac{\beta_I(\lambda_x, \lambda) E_d(0^-, \lambda_x)}{2\kappa(\lambda) + \kappa(\lambda_x)} d\lambda_x \quad (18)$$

and the in-elastic total scattering coefficient $\psi(\lambda_x, \lambda)$ (m^{-1}/nm) is defined as

$$\psi(\lambda_x, \lambda) = \int_{\Omega} \beta_I(\alpha, \lambda_x, \lambda) * d\omega \quad (19)$$

Since $\beta_I(\alpha, \lambda_x, \lambda)$ is considered isotropic, then

$$\psi(\lambda_x, \lambda) = \beta_f(\lambda_x, \lambda) * 4\pi \quad (20)$$

According to the definition of remote sensing reflectance, with Eq.18 and Eq.20, we have

$$R_{rsf}(\lambda) = I * \epsilon \int_{\lambda_x} \frac{\psi(\lambda_x, \lambda) * E_d(0^+, \lambda_x)}{[2\kappa(\lambda) + \kappa(\lambda_x)] * E_d(0^+, \lambda)} d\lambda_x \quad (21)$$

in which $\epsilon = [I + 2R]/2Q_f$.

For CDOM fluorescence, defining $\eta(\lambda_x)$ as the quantum efficiency for the emission band excited by λ_x , then^{12,13}

$$\eta(\lambda_x) = \int_{\lambda} \frac{\lambda}{\lambda_x} \frac{\psi(\lambda, \lambda_x)}{a_g(\lambda_x)} d\lambda \quad (22)$$

But $\psi(\lambda_x, \lambda)$ can be characterized by a log-normal curve²¹, so

$$\psi(\lambda_x, \lambda) = \frac{\eta(\lambda_x) * \lambda_x * a_g(\lambda_x)}{\lambda * A} * e^{-s * [\ln \frac{\lambda - \lambda_0}{\sigma}]^2} \quad (23)$$

in which

$$A = \int_{\lambda} e^{-s * [\ln \frac{\lambda - \lambda_0}{\sigma}]^2} d\lambda \quad (24)$$

where $\eta(\lambda_x)$, λ_0 , s , A and σ may vary with the type of CDOM and λ_x .

In general, $b_b \ll a$ for most oceanic waters¹⁶, so κ is close to a . For R values of about 0.05, then $\epsilon \simeq 1.1/2Q_f$. And, based on the calculation for chl-a fluorescence made by Gordon¹², the

Q_i factor for in-elastic scattering is ~ 3.7 . Then combining Eq.21 and Eq.23, the remote sensing reflectance due to CDOM fluorescence can be reduced to

$$R_{rsf}(\lambda) \doteq 0.15I * F(\lambda) \quad (25)$$

where

$$F(\lambda) = \int_{\lambda_x} \eta(\lambda_x) \frac{\lambda_x}{\lambda} \frac{a_g(\lambda_x) * E_d(0^+, \lambda_x)}{[2a(\lambda) + a(\lambda_x)] * E_d(0^+, \lambda)} * \frac{e^{-s * [\ln \frac{\lambda - \lambda_0}{\sigma}]^2}}{A} d\lambda_x \quad (26)$$

Unlike broad-band ($\sim 100\text{nm}$) CDOM fluorescence, the water Raman emission has a half-band width of about 20nm ²². Omitting this band width, i.e. assuming a narrow Raman emission, the in-elastic scattering coefficient $\psi(\lambda_x, \lambda)$ can be related to Raman scattering coefficient as

$$\psi(\lambda_x, \lambda) * d\lambda_x = b^R(\lambda_x)$$

and from Eq.21, with $\kappa \simeq a$, the remote sensing reflectance for water Raman is

$$R_{rsR}(\lambda) \doteq 0.15I * \frac{b^R(\lambda_x) * E_d(0^+, \lambda_x)}{[2a(\lambda) + a(\lambda_x)] * E_d(0^+, \lambda)} \quad (27)$$

and from the measurements of Marshall and Smith²⁰, $b^R(488) = 2.6 * 10^{-4}$.

3. MODEL

For the modeling work, a_w and b_{bm} are already known²³, and a_p and a_g can be measured or

modeled. What needs to be considered is how b_{bp} , Q , ρ , H , η , s , λ_0 , and σ change for different environments.

R_{rsR} : Since this is a type of molecular scattering, $b^R(\lambda_x)$ is considered to have a wavelength dependence similar to that of the water molecule scattering coefficient²⁴, i.e. a function of λ^{-4} . Thus $b^R(\lambda_x) = 2.6 \cdot 10^{-4} \cdot (488/\lambda_x)^4$. Then it is easy to calculate R_{rsR} using Eq. 27 when the total absorption is known. The transmittance of the air-sea interface for the solar irradiance is considered wavelength independent. The incoming light field was measured with a Licor-1800²⁵, which is used in our R_{rsR} and R_{rsf} calculation, which are begun from the excitation wavelength 300nm. The frequency shift for water Raman scattering is fixed at 3350cm^{-1} as an average from Collins et al.²²

R_{rsf} : As can be seen from Eq.26, there are at least four variables ($\eta(\lambda_x), s, \lambda_0, \sigma$) needed to calculate the remote sensing reflectance due to CDOM fluorescence when the total absorption is known. From lab measurements of CDOM fluorescence for our West Florida Shelf experiments, the quantum efficiency $\eta(\lambda_x)$ was between $\sim 0.5\%$ and $\sim 1.5\%$, and generally was rather constant for different excitation wavelengths.²¹ The slope s was about 10, $\lambda_0 \sim (.95\lambda_x - 45)$, and $\sigma \sim (195 - \lambda_x/5)$, all of which were quite constant for different stations²¹.

R_{rsb} : This value depends not only on the optical properties of the water body, but also on water depth and the bottom albedo. In the modeling work, the water depth was based on the Provisional Chart for the Gulf Coast (C&GS #1003), and the bottom albedo was based on earlier

measurements of bottom samples from near-shore, with values of 0.2 to 0.25 (used for Station 1), and from off-shore, with values from 0.4 to 0.5 (used for Stations 2 and 3). Figure 7 shows the example of those albedo spectra. The semi-diffuse attenuation coefficient $\kappa(\lambda)$ is assumed equal to total absorption $a(\lambda)$.

R_{rsw} : When using Eq. 11 to model the measured R_{rsw} , a_w , b_{bm} and total absorption $a(\lambda)$ are already known, but evaluation of b_{bp} and Q for different water bodies and solar zenith angles is required. For a_p , a_g and b_{bp} , models exist for open ocean or "Case I" waters^{5,26}, but for other areas, a_p and a_g must be measured or modeled. The particulate backscattering coefficient b_{bp} has been considered to be a spectral function of λ^{-1} or a constant for near-shore waters^{26,27}.

For the factor Q , however, there are only a few measurements, and its values have been reported from 3.2 to 12¹³. Theoretically, not much attention has been paid to factors affecting Q , perhaps because generally $L_u(\theta, \lambda, \theta, \phi)$ is considered close to Lambertian due to multiple scattering. Q has been taken to be about 4.7 and spectrally constant from 440 to 550nm²⁸, although Kirk²⁹ gives Q as ~ 4.9 , and Gordon³⁰ suggests a value of ~ 3.4 . For many studies, Q is often arbitrarily chosen as a spectral constant^{9,13,27}. From Davis' measurements (unpublished), however, Q is not spectrally constant for the waters studied in this report (Carder et al⁶), and there is a trend for Q to increase with wavelength. To model R_{rsw} for a region where b_{bp} does not covary with pigment concentration, a spectral Q factor needs to be considered, with at least four parameters are needed: two for $b_{bp}(\lambda)$, two for $Q(\lambda)$.

We consider the water-leaving radiance of the water column L_{uw} as consisting of two parts: one due to scattering by from molecules (L_{um}), and the other due to scattering by particles (L_{up}), with no interaction of scattered light between these two. Then Eq.11 can be adjusted as

$$R_{rsw} = \frac{0.33I}{a} * \left(\frac{b_{bm}}{Q_m} + \frac{b_{bp}}{Q_p} \right) * [1 - e^{-3 * D_d * a * H}] \quad (28)$$

in which Q_m and Q_p are the Q factors for molecules and particles, respectively, defined as

$$Q_m = \frac{E_{um}(0^-, \lambda)}{L_{um}(0^-, \lambda)}, Q_p = \frac{E_{up}(0^-, \lambda)}{L_{up}(0^-, \lambda)} \quad (29)$$

We are aware of neither theoretical predictions, nor experimental measurements of Q_m . However, to first order an estimate can be made based upon the phase function and illumination geometry. For a given illumination geometry, the shape of the radiance distribution within the water is determined primarily by the volume scattering function through single scattering: e.g. Gordon³¹ suggested a single-scattering approximation can be used to specify the variation of $R(\lambda)$ with the solar zenith angle, and Kirk¹⁷ used single-scattering to describe the average cosine. Combining the approach used by Jerlov³² to provide an estimation of radiance and irradiance with sun angle and depth, Austin's definition of Q factor¹⁴, and the volume scattering function of water molecules given by Morel³³, the Q_m factor for sun light was calculated (see Appendix for details). The results can be approximated by the following simple function:

$$Q_m^{sun}(j) \approx 5.92 - 3.05 \cos(j) \quad (30)$$

With the assumption that the Q_m factor due to skylight is about 3.14, the effective Q_m for a

mixture of sunlight and skylight is given by (Appendix)

$$Q_m = \frac{1 + \gamma(\lambda)}{1 + \gamma(\lambda) \frac{Q_m^{sun}(j)}{3.14}} Q_m^{sun}(j) \quad (31)$$

if we define $\gamma(\lambda) = E_d^{sky}/E_d^{sun}$, and calculate $\gamma(\lambda)$ using Gregg and Carder's model³⁴. Model results of $Q_m^{sun}(j)$ centered about 3.23 for environments studied in this contribution and are shown in Table 3.

Since we do not know the volume scattering function for the total water sample nor for the particles, b_{bp} and Q_p can not be independently estimated. However, since b_{bp} can be considered a function of $b_{bp}(400) * (400/\lambda)^n$ as in Smith and Baker²³, we may also consider Q_p to be a function of $Q_p(400) * (400/\lambda)^m$. Then b_{bp}/Q_p can be combined and modeled as $X * (400/\lambda)^Y$, where X and Y are two unknowns determined by specific particulate suites and solar illumination scenarios.

After calculating R_{rsR} , R_{rsf} and R_{rsb} , only X and Y remain as unknowns. By matching the modeled R_{rsw} and the residual of $R_{rs} - R_{rsR} - R_{rsf} - R_{rsb}$ at shorter (e.g. $\sim 400\text{nm}$) and longer (e.g. $\sim 700\text{ nm}$) wavelengths, X and Y were derived using a predictor-corrector modeling approach as in Carder and Steward¹³.

4. FIELD MEASUREMENTS

Upwelling radiance above the sea surface and downwelling sky radiance were directly measured using a Spectron Engineering spectral radiometer (model SE-590), following the method of Carder et al²⁵. Downwelling irradiance above the sea surface was measured with the SE-590 by viewing a Spectralon diffuse-reflection, calibration panel. Remote-sensing reflectance values were determined by removing reflected skylight from the upwelling radiance values^{13,25}, and dividing by the downwelling irradiance values.

The absorption coefficients for particles were obtained for surface waters following the method developed by Mitchell and Kiefer³⁵. Gelbstoff absorption a_g was derived from surface-layer K_d values determined with a Biospherical Instruments MER-1048, using the expression $a_g = k_d * \cos(j) - a_w - a_p$.

5.RESULTS AND DISCUSSION

Using the methodology described in section 3, two classes of R_{rs} are modeled: 1) Lake Tahoe with a deep, clear water column; and 2) the West Florida Shelf with shallow, gelbstoff-rich coastal waters. Figures 1-4 show the results of this approach, and Table 2 provides the latitude, longitude, approximate water depth, time/date of our experiments, and Figure 5 shows the locations of the West Florida Shelf stations. Table 3 shows the model parameters j , Q_m^{sun} , X , Y , $a_g(400)$, and $a_p(440)$ along with the measured values of $a_p(440)$ for each station. Table 4 shows the fractional contributions that R_{rsw} , R_{rsR} , R_{rsf} and R_{rsb} make to the measured R_{rs} at 440nm and

550nm.

For Lake Tahoe (Fig.1), the modeled R_{rs} curve fit the measured curve very well. From Table 4 we find that, water Raman had a bigger influence on the reflectance than did CDOM fluorescence due to low gelbstoff contributions found there. At 550nm, the influence of water Raman was over 10%, close to the 15% value for sub-surface irradiance reflectance of Marshall and Smith²⁰ and 12% value of Stavn³⁶ for 490nm. This means caution must be exercised when using this wavelength band to measure water depth for clear water bodies unless the model used includes the effects of water Raman scattering.

For West Florida Shelf Station 1 (Fig. 2), the modeled R_{rs} curve suggests a high particulate concentration (b_{bp}) and large particulate sizes for this station, since X is large and Y is small. At the same time, the bottom contribution was derived using a 13.7m water depth, a spectrally constant bottom albedo (0.20), and a CDOM fluorescence contribution with efficiency of $\eta=1.0\%$. For this station, the value of a_p required to get the best fit of the model to measured R_{rs} data was about 12% smaller than the measured a_p value. This difference, which not large, may have been, due to the errors in the optical path-length correction factor or the "beta factor"³⁷ or perhaps the package effect³⁸, especially for this inshore station. Also, the large value of $a_g(400)$ suggests that the total absorption at 440nm is dominated by a_g , making $a_p(440)$ estimates less accurate. For the offshore stations, on the other hand, modeled a_p was within $\pm 8\%$ of the measured a_p .

For Station 2, the measured R_{rs} curve (Fig. 3) is modeled using a 0.50 bottom albedo with a 25m water depth and a CDOM fluorescence efficiency $\eta=1.0\%$. For Station 3 (Fig. 4), the measured R_{rs} is modeled using 0.50 bottom albedo with a 35m water depth and a CDOM fluorescence efficiency $\eta=1.5\%$. This higher value for η is consistent with values measured for the mid-shelf region²¹. The depths required for the model are all within about $\pm 10\%$ of the chart depths without consideration of any tide influence ($< \pm 0.5\text{m}$), suggesting the utility of models such as this to remote sensing of bathymetry with high accuracy.

For the West Florida Shelf stations, the general R_{rs} model agreement with measurements is excellent, with small differences near 570nm, where the measured $R_{rs} >$ modeled R_{rs} . There are at least three possible reasons for this: a) bottom albedo uncertainties, b) phycoerythrin fluorescence³⁹, and c) water absorption coefficient uncertainty. A spectrally constant bottom albedo was used in the model; gradual spectral increases occur in the measured albedo for this region, but they could not account for the sharp increase and then decrease required for the measured and modeled R_{rs} curves to converge. More realistic explanations include the lack of a term for phycoerythrin fluorescence, and the differences in this spectral region between the reported water absorption coefficients by Smith and Baker²³ and Tam and Patel⁴⁰. Further study is required in order to resolve this issue.

Spitzer and Dirks⁴¹ made theoretical predictions regarding the contributions on the sub-surface irradiance reflectance $R(0)$ due to CDOM fluorescence. They used a Gaussian expression for fluorescence emission with wavelength and a quantum efficiency $\eta=0.0045$. Our model and

measurement work²¹ shows that the measured remote sensing reflectance can be explained in part by CDOM fluorescence, with the quantum efficiencies for the model curves twice to thrice the value 0.0045. It can be found from Table 4 that the combination of R_{rsR} , R_{rsf} and R_{rsb} can influence the ratio of $R_{rs}(440)/R_{rs}(550)$ by as much as 14%. This influence can cause a difference of $\sim 20\%$ relative to the pigment concentration determined by the power-law expression²⁶. $R_{rsw}(490)/R_{rs}^m(490)$ values as low as 0.77 were found, suggesting that great care must be taken when interpreting coastal remote sensing curves for intermediate wavelengths.

6. SUMMARY

Contributions to the water-leaving radiance signals in coastal waters of the West Florida Shelf were attributed to elastic scattering by water molecules, suspended particles, and bottom reflectance, and to in-elastic scattering by water Raman and CDOM or gelbstoff fluorescence. In-elastic scattering by pigments was not considered.

Close agreement between modeled and measured R_{rs} was achieved for all stations when all of the scattering mechanisms mentioned above were included. As much as 23% of $R_{rs}(490)$ for a station in 25m of water was attributable to water Raman, CDOM fluorescence, and bottom reflectance. CDOM fluorescence contributed about 6.3% of the signal at 440nm for a station as far as 50km offshore. This work suggests that for many applications of remote sensing in coastal waters, serious errors can occur if CDOM fluorescence and bottom reflectance are ignored, even

for stations 34 to 50 km offshore in relatively deep (25 - 36m) waters.

Appendix

Simple Estimation of $Q_m(j, \lambda)$

Following Jerlov(1976), the sub-surface upwelling irradiance $E_u^{sun}(0^-, \lambda)$ due to solar irradiance $E_d^{sun}(0, \lambda)$ on the sea-surface can be obtained by "quasi multiple-scattering," as

$$E_u^{sun}(0^-, \lambda) = E_d^{sun}(0, \lambda) \frac{\sec(j) e^{-c \sec(j)}}{c} \int_{2\pi} \frac{\beta(\alpha, \lambda) \sin(\theta)}{\sec(\theta) + \sec(j)} d\theta d\phi \quad (1)$$

where the geometry is illustrated in Figure 6. The upwelling radiance from nadir resulting from this situation is

$$L_u^{sun}(0^-, \lambda) = E_d^{sun}(0, \lambda) \frac{\beta(180-j, \lambda)}{c(\cos(j) + 1)} e^{-c \sec(j)} \quad (2)$$

in which j is the sub-surface zenith angle, c is the beam attenuation coefficient, $\beta(\alpha, \lambda)$ is the volume scattering function at wavelength λ , and

$$\cos(\alpha) = -[\cos(\Theta) * \cos(j) - \sin(\Theta) * \sin(j) * \cos(\phi)]$$

Recalling Austin's¹⁴ definition (Eq.1/Eq.2), we get

$$Q_m^{sun}(j, \lambda) = \frac{\int_{2\pi} \frac{\beta(\alpha, \lambda)}{\cos(j) + \cos(\theta)} * \cos(\theta) * d\Omega}{\frac{\beta(180-j, \lambda)}{\cos(j) + 1}} \quad (3)$$

Since $\beta(\alpha, \lambda)$ for water molecules is given by Morel³², and it is considered wavelength-independent for the visible region, the above equation can be simplified to

$$Q_m^{sun}(j) = 5.92 - 3.05 \cos(j) \quad (4)$$

Since backscattered skylight also contributes to the upwelling radiance field, and its influence on the actual $Q_m(j, \lambda)$ needs to be considered. Defining the ratio between the sub-surface downwelling sky irradiance and solar irradiance to be $\gamma(\lambda)$ and assuming the Q factor due to sky light is Lambertian or ~ 3.14 , then

$$Q_m(j, \lambda) = \frac{1 + \gamma(\lambda)}{1 + \gamma(\lambda) \frac{Q_m^{sun}(j)}{3.14}} Q_m^{sun}(j) \quad (5)$$

So, for molecular scattering, when we know the zenith angle j and the irradiance ratio $\gamma(\lambda)$ for any station, then $Q_m(j, \lambda)$ can be estimated.

7. ACKNOWLEDGEMENT

Financial support was provided by NASA through grant NAGW-465 and GSFC contract NAS5-30779, and by ONR through grant N00014-89-J-1091. Ship support was provided by the State of Florida through the Florida Institute of Oceanography. The authors wish to thank Bob Chen and Joan Hesler for administrative assistance, and Stacie Little for preparing the chart.

8. References

1. Gordon, H.R., D.K. Clark, J.L. Mueller, and W.A. Hovis, 1980, "Phytoplankton pigments from the Nimbus-7 coastal Zone Color Scanner: Comparisons with surface measurements", *Science*, 210, 63-66.
2. Carder, K.L., R.G. Steward, J.H. Paul and G.A. Vargo, 1986, "Relationships between chlorophyll and ocean color constituents as they affect remote-sensing reflectance models," *L&O*, 31(2), 403-413.
3. Morel, A., 1988, "Optical modeling of the upper ocean in relation to its biogenous matter content (Case I Waters), *JGR*, 93(C9), 10,749-10,768.
4. Carder, K.L., W.W. Gregg, D.K. Costello, K. Haddad and J.M. Prospero, 1991, "Determination of Saharan dust radiance and chlorophyll from CZCS imagery," *JGR*, 96(D3), 5369-5378.

5. Morel, A. and J.M. Andre, 1991, "Pigment distribution and primary production in the western mediterranean as derived and modeled from Coastal Zone color Scanner observations", JGR, 96(C7), 12,685-12,698.
6. Carder, K.L., S.K. Hawes, K.A. Baker, R.C. Smith, R.G. Steward and B.G. Mitchell, 1991, "Reflectance model for quantifying chlorophyll *a* in the presence of productivity degradation products," JGR, 96(C11), 20599-20611.
7. Platt, T., C. Caverhill, and S. Sathyendranath, 1991, "Basin-scale estimates of oceanic primary production by remote sensing: the north atlantic", JGR, 96(C8), 15,147-15,159.
8. Walsh, J.J., 1988, On the nature of continental shelves, Academic Press.
9. Polcyn, F.C., W.L. Brown and I.J. Sattinger, 1970, "The measurement of water depth by remote sensing techniques", Report No. 8973-26-F, Infrared and Optics Lab., Willow Run Lab., Univ. Michigan. Ann Harbor.
10. Spitzer, D., and R.W.J. Dirks, 1987, "Bottom influence on the reflectance of the sea," Int. J. Remote Sensing, 8(3), 279-290.
11. Lyzenga, D.R., 1978, "Passive remote sensing techniques for mapping water depth and bottom features", Appl. Optics, 17(3), 379-383.
12. Gordon, H.R., 1979, "Diffuse reflectance of the ocean: the theory of its augmentation by chl-a fluorescence at 685nm", Appl. Optics, 18(8), 1161-1166.
13. Carder, K.L. and R.G. Steward, 1985, "A remote sensing reflectance model of a red tide dinoflagellate off West Florida," L&O, 30(2), 286-298.
14. Austin, R.W., 1974, "Inherent spectral radiance signatures of the ocean surface," Ocean color Analysis, SIO Ref. 7410, April.

15. Gordon, H.R., O.B. Brown and M.M. Jacobs, 1975, "Computed relationship between the inherent and apparent optical properties of a flat homogeneous ocean," Appl. Optics, 14, 417-427.
16. Morel, A. and L. Prieur, 1977, "Analysis of variations in ocean color," L&O, 22(4), 709-722.
17. Kirk, J.T.O., 1991, "Volume scattering function, average cosines, and the underwater light field", L&O, 36(3), 455-467.
18. Kirk, J.T.O., 1984, "Dependence of relationship between inherent and apparent optical properties of water on solar altitude," L&O, 29(2), 350-356.
19. Morel, A. and B. Gentili, 1991, "Diffuse reflectance of oceanic waters: its dependence on sun angle as influenced by the molecular scattering contribution", Applied Optics, 30, 4427-4438.
20. Marshall, B.R. and R.C. Smith, 1990, "Raman scattering and in-water ocean properties," Appl. Optics, 29(1), 71-84.
21. Hawes, S.K., K.L. Carder, G.R. Harvey, 1992, "Quantum fluorescence efficiencies of marine humic and fulvic acids: effects on ocean color and fluorometric detection", Ocean Optics XI, Proc. SPIE. 1705: in press.
22. Collins, D.J., J.A. Bell, Ray Zanoni, I.S. McDermid, J.B., "Recent progress in the measurement of temperature and salinity by optical scattering", Ocean Optics VII, Proc. SPIE. 489, 247-269.
23. Smith, R. C. and K.S. Baker, 1981, "Optical properties of the clearest natural waters," Appl. Optics, 20(2), 177-184.

24. Stavn, Robert H. and Alan D. Weidemann, 1988, "Optical modeling of clear ocean light fields: Raman scattering effects", *Applied Optics*, 27(19), 4002-4011.
25. Carder, K.L., P. Reinersman, R.F. Chen, F. Muller-Karger, C.O. Davis, M. Hamilton, 1992, "AVIRIS calibration and application in coastal oceanic environments", G. Vane ed., Remote Sensing of the Environment, special issue on imaging spectrometry: in press.
26. Gordon, H.R. and A. Morel, 1983, "Remote assessment of ocean color for interpretation of satellite visible imagery: A review. Springer.
27. Peacock, T.G., K.L. Carder, C.O. Davis and R.G. Steward, "Effects of fluorescence and water Raman scattering on models of remote sensing reflectance," Ocean Optics X, Proc. SPIE. 1302, 303-319.
28. Austin, R.W., 1979, "Coastal zone color scanner radiometry", Ocean Optics VI, Proc. SPIE. 208, 170-177.
29. Kirk, J.T.O., 1986, Light and photosynthesis in aquatic ecosystems, Cambridge University Press.
30. Gordon, H.R., 1986, "Ocean color remote sensing: Influence of the particle phase function and solar zenith angle," *Eos Trans AGU*, 14, 1055.
31. Gordon, H.R., 1989, "Dependence of the diffuse reflectance of natural waters on the sun angle", *L&O*, 34(8), 1484-1489.
32. Jerlov, N.G., 1976, Marine Optics, Elsevier Oceanography Series, 14, Elsevier Scientific Publishing Company, Amsterdam-Oxford-New York.
33. Morel, A., 1974, "Optical properties of pure water and pure sea water," in Optical Aspects of Oceanography, ed. by N.G. Jerlov and E.S. Nielsen, 1-24, Academic, San Diego, CA.

34. Gregg, W.W. and K.L. Carder, 1990, "A simple spectral solar irradiance model for cloudless maritime atmospheres", *L&O*, 35(8), 1657-1675.
35. Mitchell, B.G. and D.A. Kiefer, 1988, "Chl-a specific absorption and fluorescence excitation spectra for light limited phytoplankton," *DSR*, 35(5), 635-663.
36. Stavn, R.H., 1990, "Raman scattering effects at the shorter visible wavelengths in clear ocean waters", *Ocean Optics X*, Proc. SPIE. 1302, 94-100.
37. Bricaud, A. and D. Stramski, 1990, "Spectral absorption coefficients of living phytoplankton and nonalgal biogenous matter: A comparison between the Peru upwelling area and the Sargasso Sea", *L&O*, 35(3), 562-582.
38. Morel, A. and A. Bricaud, 1981, "Theoretical results concerning light absorption in a discrete medium, and application to specific absorption of phytoplankton", *DSR*, 28A(11), 1375-1393.
39. Yentsch, Charles S. and Clarice M. Yentch, 1979, "fluorescence spectral signatures: the characterization of phytoplankton populations by the use of excitation and emission spectra", *J. Marine Research*, 37(3), 471-483.
40. Tam, A.C., and C.K.N. Patel, 1979, "Optical absorptions of light and heavy water by laser optoacoustic spectroscopy", *Appl. Optics*, 18(19), 3348-3358.
41. Spitzer D. and R.W.J. Dirks, 1985, "Contamination of the reflectance of natural waters by solar-induced fluorescence of dissolved organic matter", *Appl. Optics*, 24(4), 444-445.

Table 1 Symbols and units

$L_u(0^+, \lambda)$	= above-surface leaving radiance, $\text{Wm}^{-2}\text{steradian}^{-1}$
$L_{uw}(0^+, \lambda)$	= above-surface leaving radiance from water column, $\text{Wm}^{-2}\text{steradian}^{-1}$
$L_{uf}(0^+, \lambda)$	= above-surface leaving radiance from CDOM fluorescence, $\text{Wm}^{-2}\text{steradian}^{-1}$
$L_{ub}(0^+, \lambda)$	= above-surface leaving radiance from bottom reflectance, $\text{Wm}^{-2}\text{steradian}^{-1}$
$L_{uR}(0^+, \lambda)$	= above-surface leaving radiance from water Raman, $\text{Wm}^{-2}\text{steradian}^{-1}$
$L_u(0, \lambda)$	= sub-surface leaving radiance, $\text{Wm}^{-2}\text{steradian}^{-1}$
$E_u(0, \lambda)$	= sub-surface upwelling irradiance, Wm^{-2}
$E_d(0, \lambda)$	= sub-surface downwelling irradiance, Wm^{-2}
$E_d(0^+, \lambda)$	= above-surface downwelling irradiance, Wm^{-2}
$R_{rs}(\lambda)$	= remote-sensing reflectance, steradian^{-1}
$R(\lambda)$	= irradiance reflectance
ρ	= bottom albedo
H	= water depth, m
ψ	= in-elastic scattering coefficient, $\text{m}^{-1}\text{nm}^{-1}$
j	= under surface solar zenith angle, radian
K_d	= downwelling diffuse attenuation coefficient, m^{-1}
K_u	= upwelling diffuse attenuation coefficient, m^{-1}
k	= radiance attenuation coefficient for Lambertian source, m^{-1}
κ	= semi-diffuse attenuation coefficient, $a+b_b$, m^{-1}
γ	= irradiance ratio of skylight to sunlight
Q	= ratio of irradiance to radiance, steradian^{-1}

Table 2 Station locations

Station	Latitude	Longitude	water depth	Time/Date
Lake Tahoe	39°7' N	120°5' W		10.5/8-9-90
WFS St1	27°27' N	82°55' W	\approx 13.9m	10.5/3-4-90
WFS St2	27°20' N	83°03' W	\approx 24.7m	13.0/3-4-90
WFS St3	27°12' N	83°11' W	\approx 35.6m	14.9/3-4-90

Note: Time is local time. WFS = West Florida Shelf

Table 3 Model parameters for each station

Station	j	Q_m^{sun}	X	Y	$a_g(400)$	$a_p(440)$	$a_p^{mea}(440)$
Tahoe	32°	3.25	.0011	4.0	.027	.018	.017
WFS St1	35°	3.31	.0090	1.5	.170	.040	.045
WFS St2	26°	3.15	.0020	2.4	.071	.036	.035
WFS St3	27°	3.17	.0010	2.4	.068	.028	.026

TABLE 4 Optical component contributions to R_{rs}

Station		Tahoe	WFS St1	WFS St2	WFS St3
R_{rsW}/R_{rs}^m	440nm	.933	.950	.913	.864
	550nm	.890	.889	.802	.807
R_{rsJ}/R_{rs}^m	440nm	.018	.019	.029	.063
	550nm	.019	.007	.019	.038
R_{rsR}/R_{rs}^m	440nm	.035	.002	.023	.032
	550nm	.109	.004	.044	.085
R_{rsb}/R_{rs}^m	440nm		.015	.036	.017
	550nm		.096	.118	.037

Note: R_{rs}^m represents the measured remote sensing reflectance.

Captions:

Figure 1: Measured vs. modeled R_{rs} for a Lake Tahoe station

Figure 2: Measured vs. modeled R_{rs} for WFS Station 1

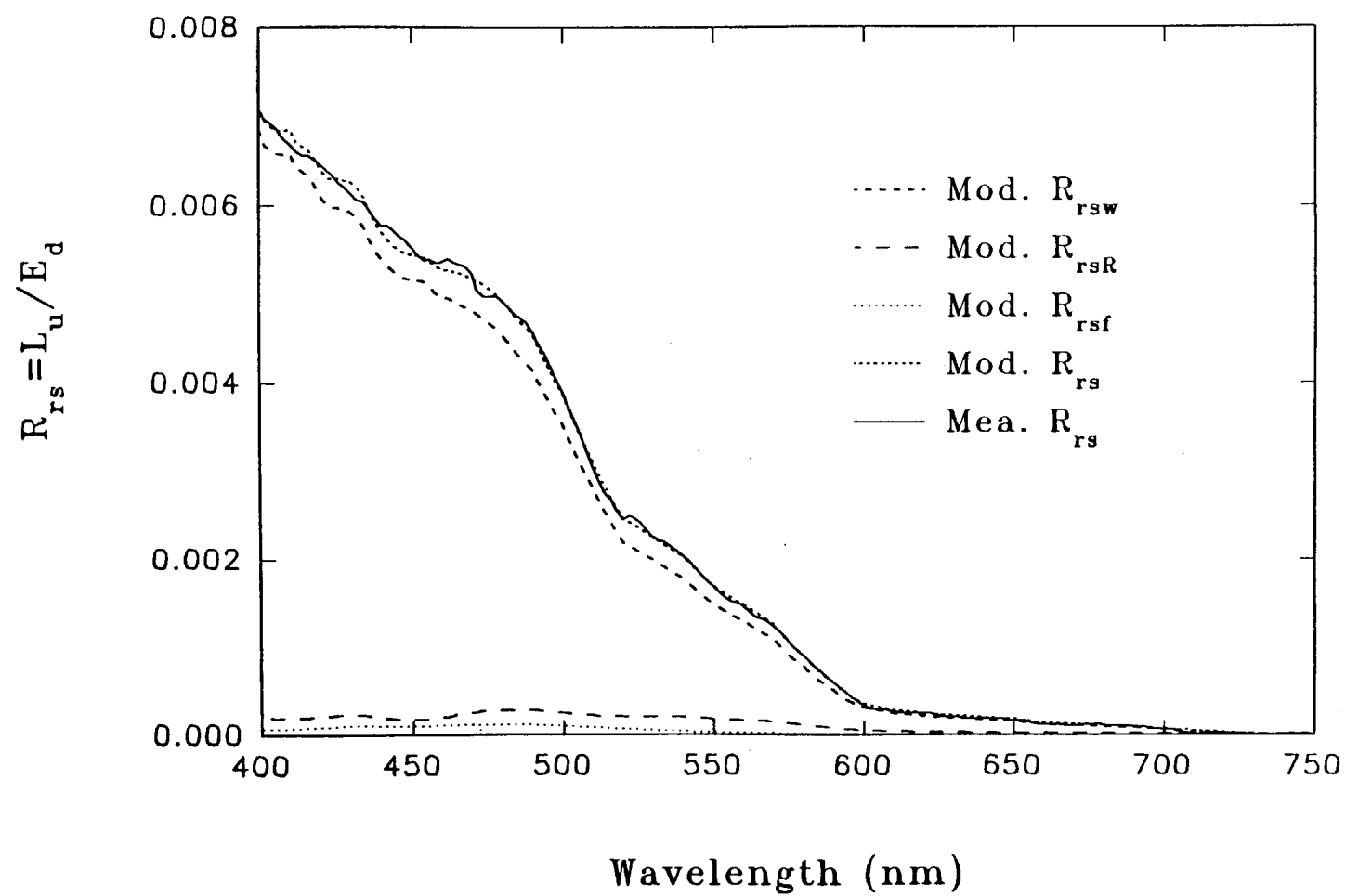
Figure 3: Measured vs. modeled R_{rs} for WFS Station 2

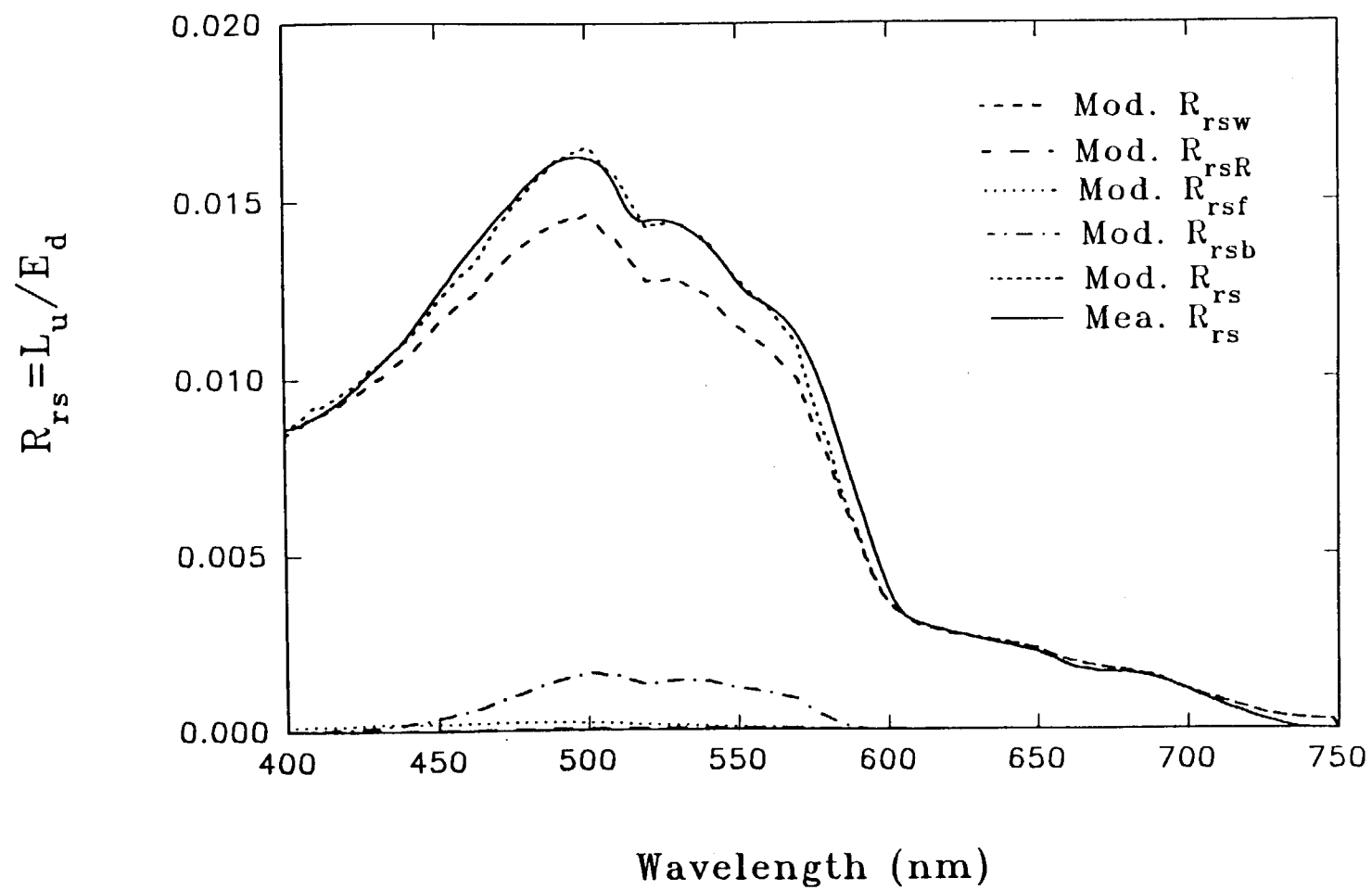
Figure 4: Measured vs. modeled R_{rs} for WFS Station 3

Figure 5: Locations for the West Florida Shelf stations

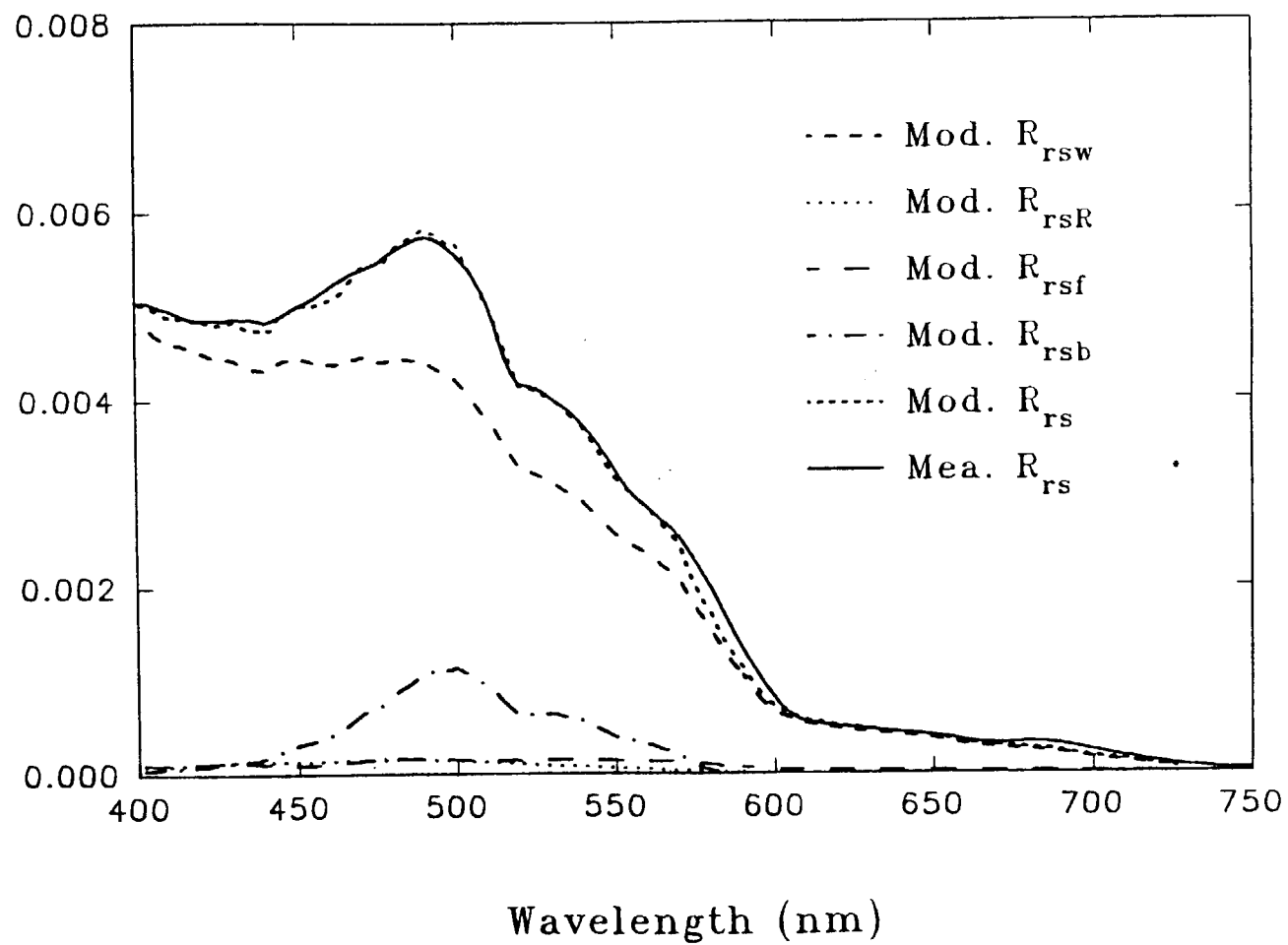
Figure 6: Illumination geometry

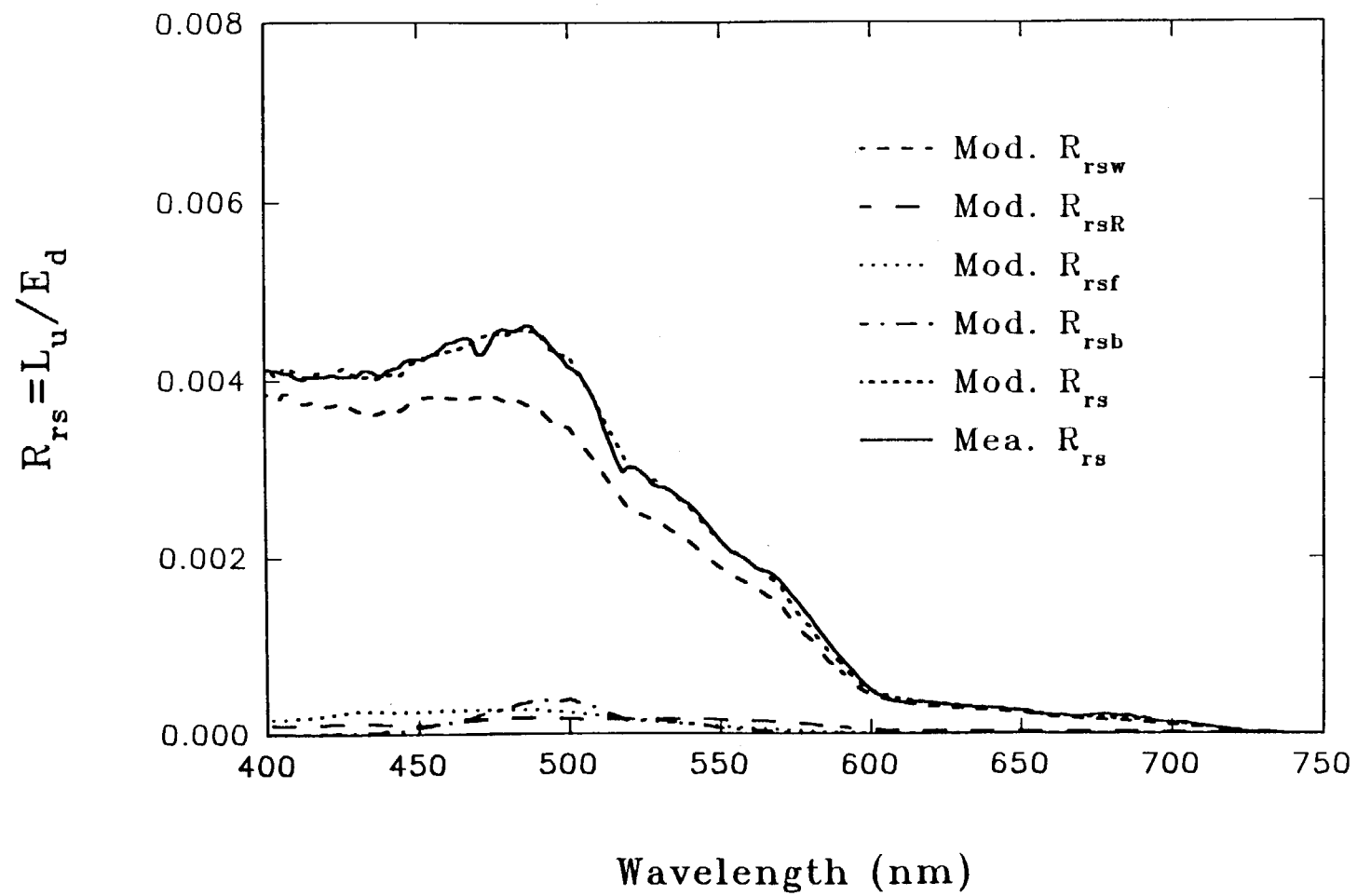
Figure 7: Bottom-albedo spectra for near-shore (dash line) and off-shore (solid line) sediments

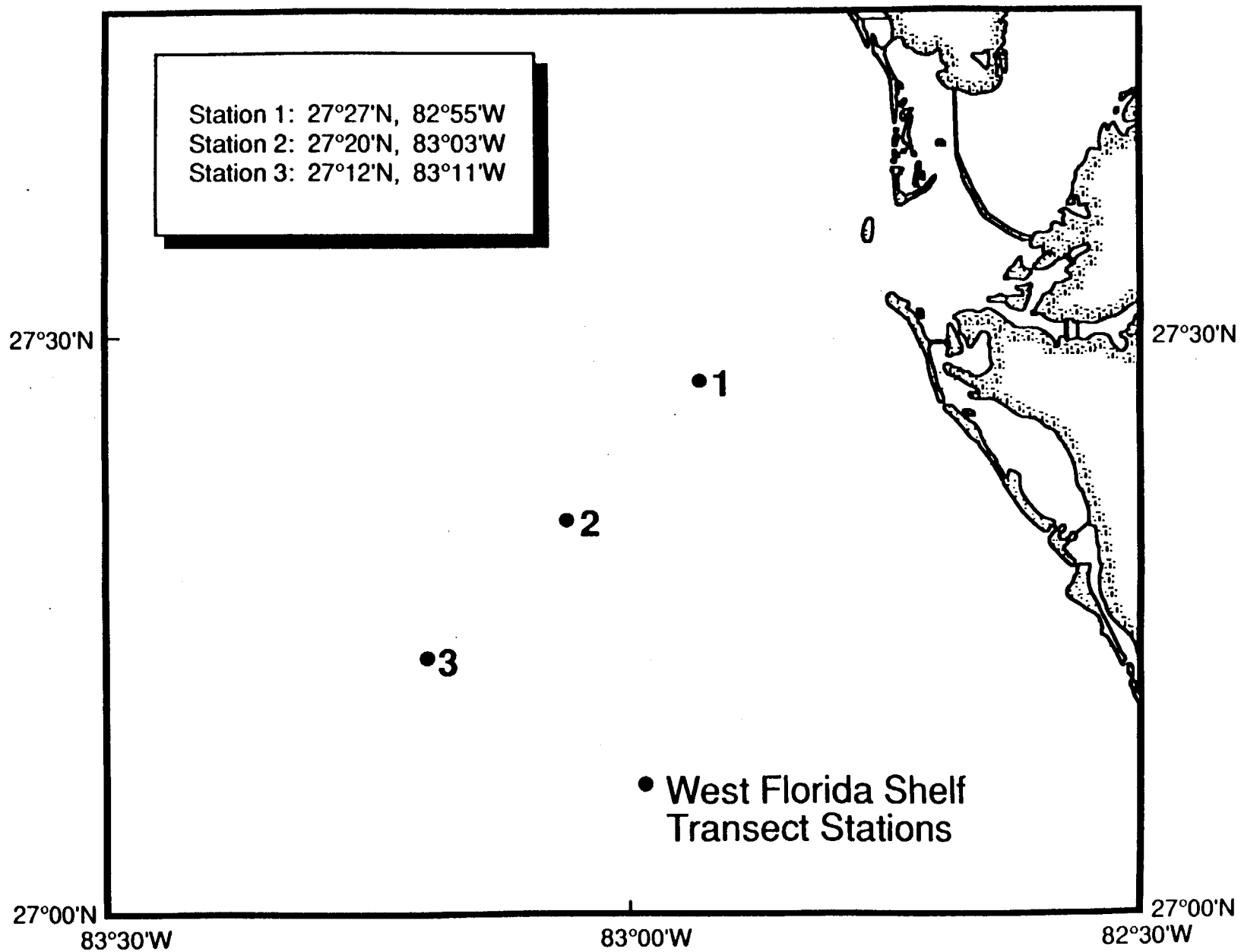




$$R_{rs} = L_u / E_d$$







The Sun

